Integrated PET/MR: Attenuation Correction and Implementation of a 16-Channel RF-Coil for Breast Imaging

Mark Oehmigen[1], Maike Lindemann[1], Titus Lanz[2], Sonja Kinner[3], and Harald H. Quick[1,4]

[1]*High Field and Hybrid MR Imaging, University Hospital Essen, Essen, Germany,* [2]*Rapid Biomedical GmbH, Rimpar, Germany,* [3]*Institute for Diagnostic and Interventional Radiology and Neuroradiology, University Hospital Essen, Essen, Germany,* [4]*Erwin L. Hahn Institute for MR Imaging, University Duisburg-Essen, Essen, Germany*

Target audience: MR Researchers and physicians who are working in the field of PET/MR hybrid imaging.

Introduction: The aim of this work is to quantify and establish a 16-channel RF coil (Rapid Biomedical GmbH, Rimpar, Germany) for clinical use [1]. Since the RF coil is located in the field-of-view (FOV) of the PET detectors during simultaneous PET/MR data acquisition, it attenuates and scatters the photons which has to be attenuation corrected (AC) for correct PET tracer activity quantification. AC of the RF coil is performed, by using a CT scan and converting the Hounsfield units (HU) to the 511 keV energy level of the PET and by creating an AC map [2]. A positioning device was designed to reposition the coil in a defined position, such that the registration of the AC map matches the coil exactly and to avoid positioning errors. To test the performance of the MR and PET features of the coil, systematic phantom test were realized. Following the validation and implementation of the AC map on the system, PET/MR examinations on four patients with breast cancer were performed and evaluated.

Material and Methods: The 16-ch breast coil was designed for an integrated whole-body PET/MR hybrid system (Biograph mMR, Siemens Healthcare, Erlangen, Germany). To create a 3D AC map of the breast coil, CT scans were performed on a dual source CT scanner (SOMATOM Definition Flash, Siemens Healthcare) with following parameters: tube voltage 140 keV, tube current 400 mA, matrix size of 512 × 512 pixels, voxel size 0.3 × 0.3 × 0.6 mm^3. For converting CT data, with an energy window level of 140 keV to the PET energy level of 511 keV, a bilinear function was used [3]. All PET data reconstructions, using the generated AC map of the RF coil and the phantoms, were performed with the reconstruction software (e7 tools, Siemens Molecular Imaging, Knoxville, USA). The software also provides the hardware AC map of the PET/MR systems patient table. For the positioning device acrylic glass providing low photon attenuation was used (Fig. 1A). Dome shaped modular PET/MR breast phantoms with a total volume of 1300 ml each where used to perform various MR, PET, and PET/MR imaging measurements (Fig. 1B). The phantoms were filled with MR signal-producing fluid (5 g NaCl per 1000 g distilled water and 3.75 g NiSO4) that was mixed with radioactive tracers to achieve simultaneous PET/MR visibility.

For performance measurements three different phantom setups were used: 1) For SNR measurements, homogenous phantoms with no insert were used. Protocol parameters were: T1-weighted 3D FLASH, FOV 400 × 400 mm², matrix size 448 × 448, 112 slices, slice thickness 1.5 mm, TR 6.04 ms, TE 2.46 ms, flip angle 10°. Also a T1 weighted 2D turbo spinecho was acquired with FOV 160 × 160 mm², matrix size 512 × 512, 20 slices with a resolution of 1 mm, TR 1780 ms, TE 15 ms, flip angle 120°. Measurements were acquired twice to create a SNR map by using the difference method [4]. 2) Spatial resolution MR measurements used a phantom insert with defined high-resolution structures made from Plexiglas [5]. The sequence parameters were identical to the SNR measurements. 3) The PET/MR insert additional to MR visible structures contains four spheres with different inner diameters of 10, 13, 17, and 22 mm, which can be filled with PET visible radiotracer. The spheres were filled with an activity concentration of 46 kBq/ml and the background had a concentration level of activity of 5.75 kBq/ml, leading to a lesion-to-background ratio of 8:1. To evaluate the accuracy of the CT-based AC map of the RF coil, the PET measurements were performed twice: 1) The RF coil was positioned on the table, homogeneous phantoms were filled with radiotracer and acquired for 30 min in listmode. 2) The RF coil was removed without repositioning the phantoms and PET data was acquired for 40 min. Subsequently, four female patients (mean age 66y ± 14y; mean BMI 27 ± 2), all diagnosed with breast cancer, were imaged using the 16-ch breast coil. Patient tissue AC was performed with MR-based image segmentation from the Dixon-VIBE sequence [6]. Hardware component AC of the patient table was performed automatically by the PET/MR system. Difference images with/out attenuation correction of the breast coil were compared to identical images where the coil was corrected retrospectively.

Results: For MR performance evaluation, SNR maps and line profiles for evaluation of spatial resolution were generated. The RF coil is capable to depict structures down to 0.2 mm with the tested setup (Fig. 2A). Homogeneous SNR distribution was achieved across the phantoms. As expected, highest SNR is perceptible in the phantom areas, where the distance to the RF coil elements is short. The relative difference map shows the effect of AC with the CT-based AC map of the breast coil. In Figure 3A the relative difference between the PET measurements with/out RF coil is shown. The mean difference is 11%; with local bias up to 27% at the periphery of the phantom, closer to attenuating structures of the RF coil. In Fig. 3B the PET measurement was re-reconstructed with the AC map of the RF coil. The mean value of the difference was reduced to -2% when applying AC of the RF coil. The patient data was corrected with a combined AC map consisting of the MR-based patient AC map, hardware component AC map of patient table, and CT-based AC map of the RF coil (Fig. 4). All four breast lesions were detected and clearly visible in the PET and PET/MR fusion images (Fig. 5 A, B). Line profiles across the breast tumor where placed to compare tracer activity with/out AC of the RF coil as exemplarily shown for one patient. The AC images in this patient showed a 12-14% higher recovered activity following AC of the RF coil (Fig. 5 C).

Discussion and Conclusion: A 16-channel RF coil for simultaneous PET/MR breast imaging has been evaluated in systematic MR, PET, and PET/MR performance tests. For integration of the RF coil into PET/MR imaging, a positioning device was developed for repeated and exact repositioning of the RF coil on the PET/MR system. A CT-based attenuation correction template of the RF coil was used to correct for photon attenuation due to the hardware components of the coil. The PET quantification bias due to RF coil attenuation was reduced from a mean difference of 11% to -2% when using the AC template. Following the results of this study, the dedicated PET/MR RF coil is now applied in PET/MR breast cancer diagnostics on patients.

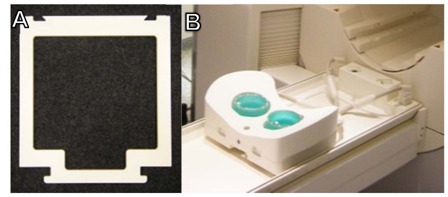

Fig. 1: Positioning device for defined z-position of the coil (A). 16-ch RF breast coil with positioning device on PET/MR systems table and with inserted breast phantoms (B).

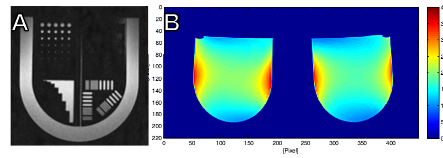

Fig. 2: MR imaging quality control with modular breast phantom: (A) high resolution structures, (B) SNR maps.

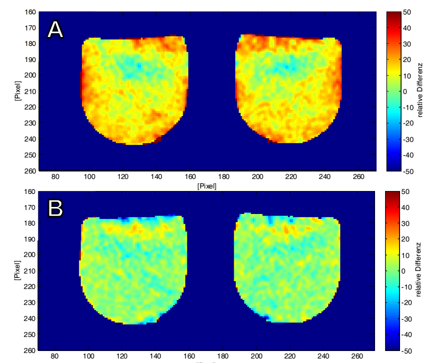

Fig. 3: PET quantification: (A) Difference images of the homogeneous filled phantoms measured with/out RF coil and without AC of the coil reveal up to 27% relative activity difference (attenuation). (B) Applying AC of the RF coil hardware components reduces the differences to a mean value of -2%.

Fig. 4: Combined umaps consisting of the MR-based umap of patient tissues, CT-based umap of the breast coil and the hardware umap of the patient table.

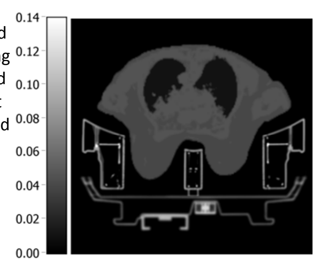

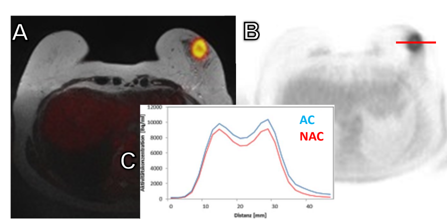

Fig. 5 (A) PET/MR fusion image, and (B) PET image of a patient with a breast tumor in the left breast The graph shows two line profiles across the tumor. The line profile in the AC image shows up to 14% higher activity (C) following AC of the RF breast coil.

References: [1] Dregerly et al., Eur Radiol. (2014); [2] Paulus et al., Med. Phys. 39 (7), 2012, 4306-4315; [3] Paulus et al., Phys. Med. Biol. 58 (2013), 8021–8040; [4] Reeder et al., Magnetic Resonance in Medicine 54 (2005); [5] Aklan et al. Med. Phys. 40 (2), 2013, 024301-11; [6] Martinez et al., J Nucl Med April 2009 vol. 50 no. 4 520-526